Adaptive Integral Inverse Kinematics Control for Lightweight Compliant Manipulators

Article *in* IEEE Robotics and Automation Letters · March 2020

DOI: 10.1109/LRA.2020.2977261

3 authors, including:

Carlos Rodríguez de Cos
KTH Royal Institute of Technology
8 PUBLICATIONS **38** CITATIONS
SEE PROFILE

J. Á. Acosta
Universidad de Sevilla
100 PUBLICATIONS **1,514** CITATIONS
SEE PROFILE

Adaptive Integral Inverse Kinematics Control for Lightweight Compliant Manipulators

C. R. de Cos*, J. Á. Acosta and A. Ollero

***Abstract*—In this paper, an adaptive to unknown stiffness algorithm for controlling low-cost lightweight compliant manipulators is presented. The proposed strategy is based on the well-known transpose inverse kinematics approach, that has been enhanced with an integral action and an update law for the unknown stiffness of the compliant links, making it valid for soft materials. Moreover, the algorithm is proven to guarantee global task-space regulation of the end effector. This approach has been implemented on a very low-cost robotic manipulator setup (comprised of 4 actuated and 3 flexible links) equipped with a simple Arduino board running at 27Hz. Notwithstanding, the strategy is capable of achieving a first-order-like response when undisturbed, and recover from overshoots provided by unforeseen impacts, smoothly returning to its nominal behaviour. Moreover, the adaptive capabilities are also used to perform contact tasks, achieving zero steady-state error. The tracking performance and disturbance rejection capabilities are demonstrated with both theoretical and experimental results.**

***Index Terms*—Robust/Adaptive Control of Robotic Systems; Compliance and Impedance Control; Aerial Systems: Mechanics and Control**

I. Introduction

In the recent years, the interest on lightweight compliant manipulators has grown due to their potential for applications with limited payloads, such as Aerial Manipulation [1]–[3] and Human-Robot Interaction [4]–[7]. Compliant robot manipulators (RM henceforth) are known for exhibiting safe contact behaviour by means of force/impedance control (see [8]–[10]) and collision detection (see [11], [12]), among others, being a solid option for autonomous inspection (see [13] and references therein). However, when compared with rigid RMs in terms of tracking performance, their good compliant behaviour comes on the cost of worsening that error tracking, mainly due to a much more complex internal dynamics induced by the flexible modes. On the other hand, the flexible ones achieve compliance by mechanical design unlike the rigid ones that can only do it by feedback. Among others, this drawback results in higher sensitivity to control delays, mistuning and slow transients to maintain the closed-loop stability. The most common approach to minimise those effects is with a thorough mechanical design that improves the performance of the system, thus providing a trade-off solution between compliant oscillations and end-effector (EE henceforth) time convergence (see [14], [15]).

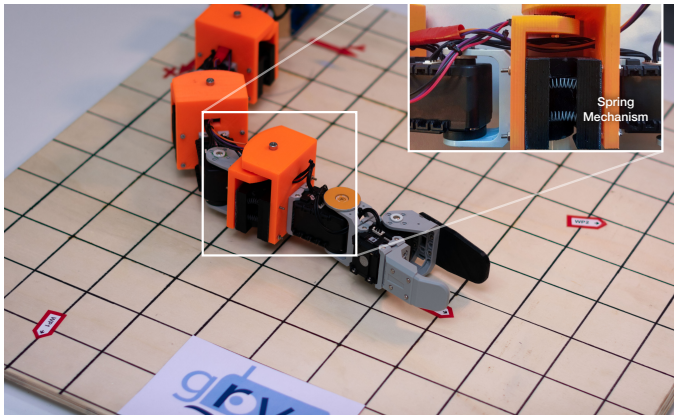

Fig. 1. Lightweight compliant manipulator used for demonstration sliding over the supporting surface (where waypoints are highlighted by directional markers) with detail of the flexible links.

The main motivation for this line of research has been the application of aerial manipulation in industrial environments, that is addressed in the AEROARMS project [16]. Among the applications within this project, two of the most demanding scenarios for manipulation involve: i) the inspection through contact with pipeline coatings, including materials with non-linear mechanical properties, very troublesome to measure and dependent on the environmental conditions (see [17] and [18], respectively); and ii) impact of the EE during the operation with unexpected elements [13], [19]. The experiments carried out in those scenarios evinced the need for control solutions in lightweight RMs with the following requirements: to be capable of handling compliance under force-contact overshoots; enhanced rejection capabilities under external disturbances and delays; to avoid incidents in hazardous environments (outdoors); and low computational demands to prolong the duration of the missions.

Therefore, the main contribution of this paper is a control strategy for lightweight RMs able to reduce the negative effects of compliance on error tracking performance and with disturbance rejection capabilities, while preserving their inherent safety of the platform under the impacts of inspection. In this way, the proposed algorithm framework is the closed-loop inverse kinematics (IK henceforth) approach, due to their reliability and good performance exhibited in rigid RMs with servomotors (see e.g. [20]–[22]). Thus, we took as a starting point the robust closed-loop IK controller designed by some

Manuscript received: September, 10, 2019; Revised November, 16, 2019; Accepted February, 4, 2020.

This paper was recommended for publication by Editor Paolo Rocco upon evaluation of the Associate Editor and Reviewers' comments. This work was supported by the AEROARMS project of the EU Horizon 2020 programme under grant agreement No 644271 and the research activities of C.R. de Cos by the VPPI of the University of Seville.

*Corresponding author.

The authors are with the GRVC Robotics Laboratory, Universidad de Sevilla, Camino de los Descubrimientos s.n., 41092 Sevilla, Spain. (email: {crdecos,jaar,aollero}@us.es).

Digital Object Identifier (DOI): see top of this page.

of the authors in [22] for rigid RMs. The main contributions of the control algorithm cover the aforementioned requirements as follows:

i) a far-from-trivial extension of the robust IK algorithm [22] to cope with compliant RMs, yielding a nonlinear and adaptive PI controller, unlike the linear PI in [22];
ii) enhancing the strategy with an adaptive update law for the unknown stiffness of the compliant links, making the approach valid for soft materials; and
iii) requiring low computational demand, as demonstrated by the experiments carried out with a basic computer.

These contributions improve the existent IK solutions for flexible links. In comparison, e.g. in [23], [24] the stiffness must be known and, the adaptive solutions for industrial RMs in [25], [26] need high computational capabilities. Moreover, the proposed approach relies on the Jacobian transpose avoiding large control inputs troublesome near to singularities of (pseudo) inverse approaches (see [27], [28]).

Remark 1. *For the sake of clarity, it is worth explaining the use of the terms 'compliance' and 'safety' throughout the article. As aforementioned, the proposed approach is motivated by the inspection through contact in industrial environments. While in the soft interactions with humans safety means prevention of damage to them, in this approach safety means a hazardous situation for the aerial manipulation platform while flying, like unexpected impacts. Accordingly, what we consider compliance in this scenario is the ability of accommodating itself under these impacts coming from the inspection while preserving the tracking performance. The reason why we use the word compliance, and not disturbance rejection, is that the proposed algorithm makes the system behave by absorbing impacts and then it follows its target. A better term to define the overall behaviour of the aerial manipulator under impacts, could be 'resilience'. We refer readers to the thorough work in [29], where the authors clarify and analyse in depth that in case of requiring a soft contact –like with humans–, the target of the controller cannot be strict error tracking.*

The paper is structured as follows: Section II outlines the background needed to introduce the control solution presented in Section III with its stability results in Section IV; Section V is devoted to characterising the benchmark application and the experimental settings and results. Finally, the paper is wrapped up with a conclusion Section.

Notation: the operator col$(\cdot)$ denotes the concatenation of the vectors in the argument into a column vector; $|\cdot|$ stands for vector norms, with $|\cdot|_P$ vector norms weighted by the matrix P; and $||\cdot||_P$ denotes matrix norms. The Kernel or Nullspace of $(\cdot)$ is denoted as $\ker(\cdot)$.

Acronyms: RM – Robot Manipulator, AM – Aerial Manipulator, CG – Centre of Gravity, DoF – Degrees of Freedom, EE – End-Effector, IK – Inverse Kinematics, UAV – Unmanned Aerial Vehicle.

II. Background and Framework

Consider a RM task space of dimension S and let us denote the EE position as $p := \text{col}(\bar{p}, \bar{\alpha}) \in \mathbb{R}^S$, being

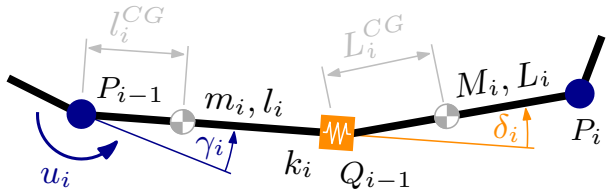

Fig. 2. Actuated and flexible angular DoF of the RM, with P_k and Q_k the actuated and flexible link positions (definitions of parameters in the text).

$\bar{p} \in \mathbb{R}^{S_p}$ and $\bar{\alpha} \in \mathbb{R}^{S_\alpha}$ its Cartesian position and orientation, respectively. The joint space is comprised of N rotation degrees of freedom (DoF henceforth) actuated by servomotors, γ, and M compliant (flexible) deflections, δ (see Fig. 2), and let its configuration be denoted as $q = \text{col}(\gamma, \delta) \in \mathbb{R}^{N+M}$. Accordingly, the velocity vector can be split through their corresponding translation and revolution Jacobians as

$$\dot{p} = J_\gamma \dot{\gamma} + J_\delta \dot{\delta} = \begin{pmatrix} J_\gamma^t & J_\delta^t \\ J_\gamma^r & J_\delta^r \end{pmatrix} \dot{q} = J_q \dot{q}, \tag{1}$$

being $J_\gamma^t \in \mathbb{R}^{S_p \times N}$, $J_\delta^t \in \mathbb{R}^{S_p \times M}$ the translational Jacobians, and $J_\gamma^\alpha \in \mathbb{R}^{S_\alpha \times N}$, $J_\delta^\alpha \in \mathbb{R}^{S_\alpha \times M}$ the rotational ones, with respect to the actuated, γ, and compliant, δ, DoF. Then, the dynamics are written by means of the Lagrange equations as

$$B\ddot{q} + C\dot{q} + Kq = u + u_{EE} + g,$$

with $B(q), C(q, \dot{q})$ the inertia and Coriolis terms matrices; $u := \text{col}(\tau, \varnothing_{M\times 1}) \in \mathbb{R}^{N+M}$ the RM control inputs with $\tau \in \mathbb{R}^N$ the servo torques; $u_{EE} := \text{col}(J_\gamma^\top f^{EE}, J_\delta^\top f^{EE}) \in \mathbb{R}^{N+M}$ the EE-applied external forces; and g:=col$(J_{CG,\gamma}^\top m g_0, J_{CG,\delta}^\top m g_0) \in \mathbb{R}^{N+M}$ the gravitational terms applied in the Center of Gravity (CG henceforth). Among these definitions, f^{EE} stands for the EE contact force; $J_{CG,\gamma}, J_{CG,\delta}$ for the manipulator CG Jacobians with respect to both sets of angles (see [28]); m for the mass of the RM; g_0 for the gravity acceleration vector in the inertial reference frame; and K for the system stiffness matrix given by

$$K = \begin{pmatrix} \varnothing_{N\times N} & \varnothing_{N\times M} \\ \varnothing_{M\times N} & K_\delta \end{pmatrix},$$

where the stiffness of the compliant links is given by the submatrix $K_\delta \in \mathbb{R}^{M\times M}$ (see e.g. [28]).

III. Adaptive Integral IK Nonlinear Control

The main contribution of the paper is a nonlinear and adaptive control strategy that considers the kinematics of the flexible links with measured deflections and copes with the unknown stiffness of the flexible links. To do so, an adaptive estimation of their stiffness is used to modify the rigid arm Jacobian, from which the commanded angular speeds are obtained, as presented in Fig. 3. In Fig. 3 we have tried to compare with standard inverse kinematics algorithms. Thus, the bottom feedback loop it could be considered similar (but nonlinear) to the standard one, and at the top, the block estimating the stiffness and updating the core algorithm. To start with, we use the slow time-varying approach proposed

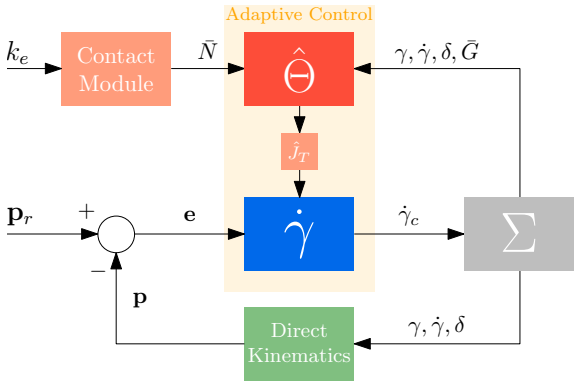

Fig. 3. Control closed-loop block schematic with: the actuation considering the flexibility of the RM (in blue), the adaptive estimation of the flexible links kinematics (in orange) and the direct kinematics (in green).

in [24], that yields a pseudo-static formulation with elastic contact, to provide an explicit estimate of the flexible link speeds. This formulation reads

$$K_\delta \delta = J_\delta^{t\top} f^{EE} + J_{CG,\delta}^\top m g_0, \tag{2}$$

with $f^{EE} = -k_e n n^\top (\bar{p} - \bar{p}_s)$ the force on the EE and $k_e \in \mathbb{R}$ the elastic constant of the material to push, both unknown; $n \in \mathbb{R}^{S_p}$ the outward normal at the contact point and $\bar{p}_s \in \mathbb{R}^{S_p}$ the surface contact point while undeformed (see Fig. 4). Then, by deriving (2), the deflection speeds are estimated as

$$K_\delta \dot{\delta} = \left[-k_e \left(\frac{\partial J_\delta^{t\top}}{\partial \gamma} \bar{N} + J_\delta^{t\top} n n^\top J_\gamma^t \right) + \frac{\partial J_{CG,\delta}^\top}{\partial \gamma} m \bar{G} \right] \dot{\gamma}, \tag{3}$$

being the EE and CG extended derivative Jacobian matrices defined block-wise as

$$\begin{aligned} \frac{\partial J_\delta^{t\top}}{\partial \gamma} &:= \left(\frac{\partial J_\delta^{t\top}}{\partial \gamma_1} \quad \cdots \quad \frac{\partial J_\delta^{t\top}}{\partial \gamma_N} \right), \\ \frac{\partial J_{CG,\delta}^\top}{\partial \gamma} &:= \left(\frac{\partial J_{CG,\delta}^\top}{\partial \gamma_1} \quad \cdots \quad \frac{\partial J_{CG\delta}^\top}{\partial \gamma_N} \right), \end{aligned}$$

and the extended matrices $\bar{N}, \bar{G} \in \mathbb{R}^{NS_p \times N}$ column-wise as $\bar{N}_j := \mathrm{col}(\varnothing_{(j-1)S_p}, \, n n^\top (\bar{p} - \bar{p}_s), \, \varnothing_{(N-j)S_p})$ and $\bar{G}_j := \mathrm{col}(\varnothing_{(j-1)S_p}, \, g_0, \, \varnothing_{(N-j)S_p})$ to simplify the notation.

This estimation of the deflection speeds allows us to define the stiffness parametrisation for the deflection kinematics, which will be used for the adaptive solution, via the uncertain matrix $\Theta := (k_e K_\delta^{-1}; K_\delta^{-1}) \in \mathbb{R}^{2M \times M}$, assumed constant or slow time-varying, and then (3) becomes

$$\dot{\tilde{\delta}} = -\Theta^\top J_{fg} \dot{\gamma}, \tag{4}$$

where $J_{fg} \in \mathbb{R}^{2M \times N}$ represents the Jacobian of the external forces applied on the RM and given by

$$J_{fg} = \begin{pmatrix} \dfrac{\partial J_\delta^{t\top}}{\partial \gamma} \bar{N} + J_\delta^{t\top} n n^\top J_\gamma^p \\ -\dfrac{\partial J_{CG,\delta}^\top}{\partial \gamma} m \bar{G} \end{pmatrix}.$$

Then, upon defining the stiffness errors as $\tilde{\Theta} := \Theta - \hat{\Theta}$, the EE kinematics in (1) can be reformulated using (4) as

$$\dot{p} = \Big(\underbrace{\hat{J}_T(q, \hat{\Theta})}_{\text{Estimate}} - \underbrace{J_\delta \tilde{\Theta}^\top J_{fg}}_{\text{Uncertain}} \Big) \dot{\gamma}, \tag{5}$$

where $\hat{J}_T \in \mathbb{R}^{S \times N}$ is the equivalent Jacobian needed to take into account the flexible links kinematics, defined as

$$\hat{J}_T(q, \hat{\Theta}) := J_\gamma - J_\delta \hat{\Theta}^\top J_{fg}, = J_q J_{\hat{\Theta}}, \tag{6}$$

with matrices $J_\Theta, J_{\hat{\Theta}} \in \mathbb{R}^{(N+M) \times N}$ given by

$$J_\Theta := \begin{pmatrix} I_N \\ \Theta^\top J_{fg} \end{pmatrix}, \; J_{\hat{\Theta}} := \begin{pmatrix} I_N \\ \hat{\Theta}^\top J_{fg} \end{pmatrix}. \tag{7}$$

Remark 2. *As it is well known in adaptive control, a linear and multiplicative parametrisation of the uncertainty is essential. Thus, the involved non-trivial definitions made above allow us to factor the uncertain parameters with the nonlinear terms in (4), thus allowing to construct an additive error in the highly nonlinear kinematics given by (5).*

Let then $e := p_r - p \in \mathbb{R}^S$ be the EE position and orientation error, p_r its associated reference, and $\xi \in \mathbb{R}^S$ a term assimilable to the integral of the error. Finally, the proposed adaptive and nonlinear controller based on this equivalent Jacobian reads

$$\dot{\xi} = K_I \hat{J}_T K_\gamma \hat{J}_T^\top K_P \, e - K_\xi \xi, \tag{8}$$

$$\dot{\gamma} = K_\gamma \hat{J}_T^\top \left(K_P e + K_I \xi \right), \tag{9}$$

$$\dot{\hat{\Theta}} = \varpi(q, e, \dot{\gamma}), \tag{10}$$

where the gain matrices $K_\xi, K_P \in \mathbb{R}^{S \times S}$ and $K_\gamma \in \mathbb{R}^{N \times N}$ are positive definite and $K_I \in \mathbb{R}^{S \times S}$ is non singular. The adaptive stiffness function $\varpi \in \mathbb{R}^{2M \times M}$ is not yet defined.

Remark 3. *It is interesting to underscore the nonlinear nature of the Proportional Integral action in (9) due to the nonlinear integral-like error term formulation in (8), essential to add robustness and to guarantee zero steady-state error and to the interlaced Jacobian matrix (6).*

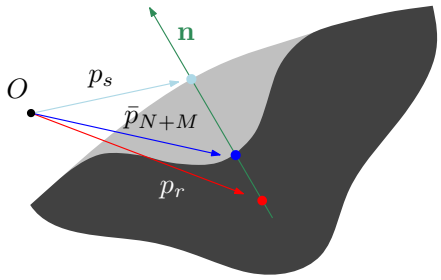

Fig. 4. Definition of the contact parameters, with undeformed (light gray) and deformed (dark gray) bodies, together with the contact normal.

IV. Main Stability Result

In the following proposition, we complete the proposed strategy and establish its stability and robustness properties including the uncertain dynamics behaviour.

Proposition 1. *Consider the uncertain system (5) for any $N \geq S$ and assume $\text{rank}(J_q) = S$, along with the adaptive-state feedback given by (8)–(10) and the update law*

$$\varpi(q, e, \dot{\gamma}) := \Gamma J_{fg} \dot{\gamma}\ e^\top K_P J_\delta, \tag{11}$$

with $\Gamma \in \mathbb{R}^{2M \times 2M}$ a positive definite gain matrix. Then, the closed-loop inverse kinematic system for $\dot{p}_r = 0$ becomes

$$\begin{bmatrix} \dot{\xi} \\ \dot{e} \end{bmatrix} = \begin{bmatrix} -K_\xi & K_I \hat{\mathcal{J}} K_P \\ -\hat{\mathcal{J}} K_I & -\hat{\mathcal{J}} K_P \end{bmatrix} \begin{bmatrix} \xi \\ e \end{bmatrix} + \begin{bmatrix} 0 \\ J_\delta \tilde{\Theta}^\top J_{fg} \dot{\gamma} \end{bmatrix}, \tag{12}$$

with $\hat{\mathcal{J}} := \hat{J}_T K_\gamma \hat{J}_T^\top$. Moreover, the zero equilibrium of (12), together with (10)–(11), is (globally) asymptotically stable.

Proof. The first claim is straightforward recalling the definition of the EE error and combining it with (5), (8) and (9). For the second one, let us define the radially unbounded and positive definite Lyapunov function candidate as

$$V := \frac{1}{2}|e|^2_{K_P} + \frac{1}{2}|\xi|^2 + \text{Tr}\left(||\tilde{\Theta}||^2_{\Gamma^{-1}}\right).$$

Its time derivative along the system trajectories (12) becomes

$$\begin{aligned} \dot{V} &= e^\top K_P\ \dot{e} + \xi^\top \dot{\xi} + \text{Tr}\left(\tilde{\Theta}^\top \Gamma^{-1} \dot{\tilde{\Theta}}\right) \\ &= -e^\top K_P \hat{\mathcal{J}} K_P\ e - \xi^\top K_\xi\ \xi \\ &\quad + e^\top K_P J_\delta \tilde{\Theta}^\top J_{fg} \dot{\gamma} - \text{Tr}\left(\tilde{\Theta}^\top \Gamma^{-1} \dot{\hat{\Theta}}\right) \\ &= -e^\top K_P \hat{\mathcal{J}} K_P\ e - \xi^\top K_\xi\ \xi \\ &\quad + \text{Tr}\left[\tilde{\Theta}^\top \left(J_{fg} \dot{\gamma}\ e^\top K_P J_\delta - \Gamma^{-1} \dot{\hat{\Theta}}\right)\right], \end{aligned}$$

where the last term is cancelled out with (10)–(11). Since V is positive definite, $\dot{V} \leq 0$, and the closed-loop system is autonomous, we can then invoke LaSalle's Invariance Principle. For that, we need to analyse the largest invariant set included in the residual set given by $\dot{V} = 0$ that reads

$$\Omega := \left\{(e, \xi) \in \mathbb{R}^{2S} : \hat{J}_T^\top K_P\ e = 0, \xi = 0\right\}.$$

To this end, let us define $\bar{e} := K_P\ e$ and notice that the residual dynamics in Ω become $\dot{e} = \dot{\xi} = \dot{\gamma} = \dot{\hat{\Theta}} = 0$. Hence, the largest invariant set is only comprised of fixed points (equilibria), reducing the analysis to rule out all the non desired equilibria. Notice that $\hat{J}_T^\top \bar{e} = 0$ is equivalent to $\bar{e} \in \ker(\hat{J}_T^\top)$. Thus, $\hat{J}_T^\top \bar{e} = 0$ has the unique trivial solution if and only if, $\ker(\hat{J}_T^\top) = \emptyset \Leftrightarrow \text{rank}(\hat{J}_T^\top) = S$. Recall from (7) that $\text{rank}(J_{\hat{\Theta}}^\top) = N$, by assumption that $\text{rank}(J_q^\top) = S$ and by design $N \geq S$. Therefore, $\text{rank}(\hat{J}_T^\top) = \text{rank}(J_{\hat{\Theta}}^\top J_q^\top) \leq \min\{N, S\} = S$, concluding the proof. □

Remark 4. *The stability result of Proposition 1 relies on the assumption of a full-rank Jacobian J_q, that can be overcome by design. The RM chosen for the experiments, as well as other similar designs in [28], fulfils this characteristic.*

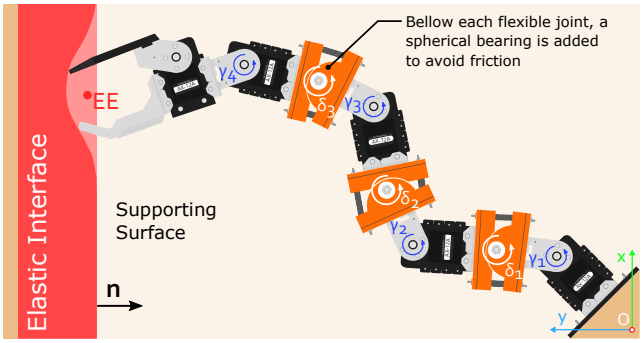

Fig. 5. Benchmark RM with reference frame, DoF, contact normal and supporting surface, being the friction with the latter considered negligible due to the use of spherical bearings below the flexible joints.

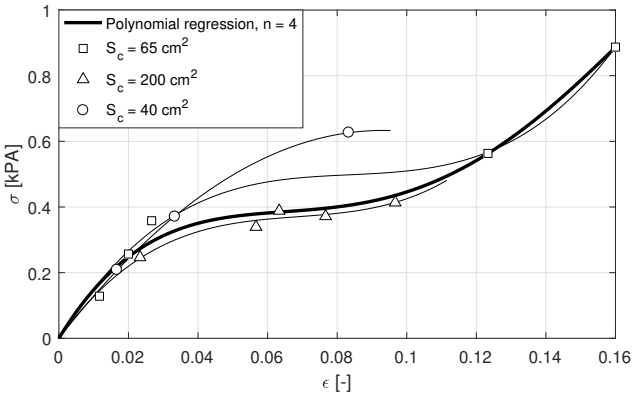

Fig. 6. Preliminary identification of the stress-strain curve for the foam used in the benchmark application, with S_c the cross-sectional area of the specimen and L_c = 0.3 m its length.

TABLE I
Benchmark Application Parameters

Compound joints [cm, g, N m rad^{-1}]							EE joint [cm, g]		
l	L	l^{CG}	L^{CG}	m	M	k	l_{EE}	l_{EE}^{CG}	m_{EE}
4.8	6.2	2.4	3.6	25	64	0.8	12.0	6.0	72

TABLE II
Benchmark Control Gains

$K_P^{\bar{p}}$	$K_P^{\bar{\alpha}}$	$K_I^{\bar{p}}$	$K_I^{\bar{\alpha}}$	K_ξ	Γ_1	Γ_2	Γ_3
98.40	2.40	0.35	0.30	20.00	0.04	0.07	0.12

Remark 5. *It is worth noting that the numerical computation of the whole algorithm (8)–(11) does not involve any matrix inverse calculation. Accordingly, in the case of implementing it in an RM passing through singular configurations, the response near them will not provide unbounded inputs and it will rest at a stable configuration.*

V. Experimental Results

To validate the proposed control strategy, the low-cost planar RM depicted in Fig. 5 is used (see [30]). It consists of 4 actuated and 3 compliant DoF with a planar design (thus reducing the load of matrix calculations) and whose links are identical except for the last one (EE) (see Table I). The control

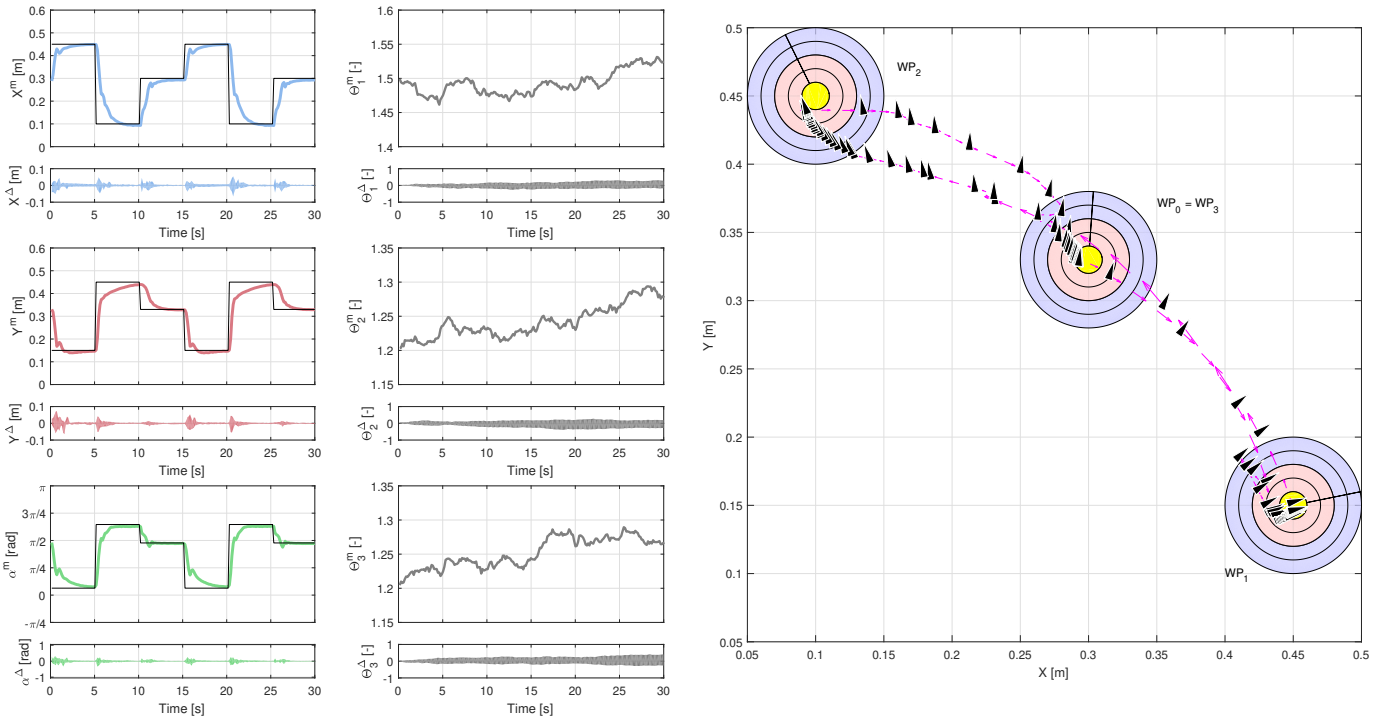

Fig. 7. On the left, mean EE position and reference (in colours), and adaptive parameters (in gray), for the set of consecutive experiments both as a function of time, with maximum deviations from the set mean denoted by $(\cdot)^{\Delta}$. On the right, XY plane with orientation and position indicated by black arrows, speed as magenta arrows and waypoints as targets with annuli of 1 cm of separation and reference orientation as black radii.

gains used in the experiments are shown in Table II, except for K_γ, chosen equal to the identity matrix size 4.

The servos used are the Dynamixel AX-12A [31]. Among their main features, the resolution of $0.3°$ ($5.236 \cdot 10^{-3}$ rad), the stall torque of 1.5 N·m and a no-load speed of 59 RPM stand out. Moreover, as the servos are incompatible with speed control for this application, two options arisen: using the continuous speed mode or an ad-hoc angular position solution. The latter is chosen due to the high-speed wheel-like motion of the first, modifying the algorithm to make use of the superposition of angular speed profiles. Secondly, the flexible joints consist of a double spring system with low stiffness, being this property a design decision. As a result, the compliant links tend to reach the limit of their operational range, and are prone to significant oscillations when the RM is actuated. Both situations, however, are chosen to highlight the capabilities of the control solution in a ill-conditioned scenario. To measure these deflections, the Murata SV01 rotatory position potentiometers are embedded in the flexible joints. Finally, the calculations are carried out by an Arbotix-M Robocontroller [32], with a 16 MHz AVR microcontroller and compatibility with the Arbotix actuators. There have been two main limitations of this low-cost board: 1) the lack of memory prevented the implementation of the gravitational terms, thus choosing a planar design for the RM (implementing them is about doubling the code lines); 2) the proposed controller is running at a frequency of 27Hz ($\pm$2Hz). For the latter, as higher sampling frequencies generally imply a better performance in controllers designed in continuous time, this low sample frequency highlights its robustness.

Remark 6. *A preliminary analysis was conducted to determine the best experimental setting achievable with the aforementioned computer board. The results obtained, based on the computational complexity of the algorithms involved, showed that: i) using the controller in the benchmark application but with S = 6 would roughly doubled the computational cost; and ii) the core of the algorithm needed twice as much time as a controller using the damped least-squares inverse (DLS) without considering the flexible nature of the manipulator in any way. Moreover, we estimate that for a realistic 6D RM (N=7, M=4), the computational cost would only quadruple the one of the planar benchmark application. Furthermore, comparing this result with the DLS-based solution, we obtain that the expected difference is limited to about 30% and, therefore, the proposed approach also shows a good scalability.*

Three scenarios focused on the rejection capabilities of the solution are chosen for the benchmark application: i) tracking without external disturbances, ii) impact with unexpected external elements, and iii) contact with an interface whose nonlinear behaviour is also unknown (see Fig. 5 and Fig. 6). Attached to the paper, videos and dataset files of the experiments are included.[1]

Firstly, a set of 13 consecutive undisturbed experiments is carried out (Fig. 7), obtaining a mean first-order-like response under step references without significant variations between experiments. Associated with this, the adaptive parameters evolve in mean, having peaks in their values at the reference steps and showing important variations among the sample due

[1]For an enhanced version see https://youtu.be/fP3HrJ0x37k in the GRVC YouTube channel.

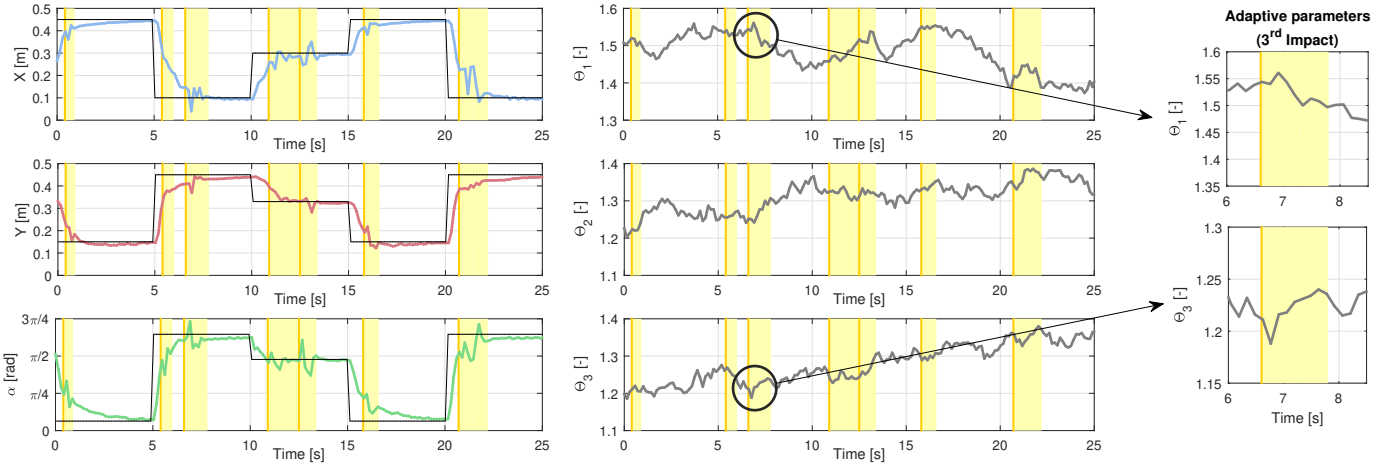

Fig. 8. EE position and adaptive parameters for multiple impacts (vertical yellow lines), highlighting associated transients (transparent yellow rectangles), with a detail of the response of the adaptive extension on the right.

to the white noise added to increase the adaptive reactivity. Moreover, a XY-plane representation of the mean experiment is also included in Fig. 7 to further illustrate the convergence of the solution.

Secondly, the results of the impact scenario enrich our understanding of the disturbance rejection capabilities. As depicted in Fig. 8, the RM is hit 7 times in arbitrary directions and intensities during the experiment, recovering stability after all these situations. This is achieved by using the accommodation capabilities of the adaptive solution, responding after each impact with a sudden change of their tendency (as with Θ_3 in the second impact), or with a noticeable peak in some of the adaptive parameters (such as in the third impact). Afterwards, the RM controller shows the same first-order-like response previously mentioned. Additionally, it is also worth noting that even for impacts during the accommodation transient (such as the one induced at 22 s) or multiple impacts (such as at 11 s), the solution is capable of recovering its undisturbed behaviour.

Finally, the contact results of the solution are shown in Fig. 9. This scenario is focused on the contributions of the adaptive solution to the permanent regime response of the RM with contact. In this case, a non-elastic material –i.e. the stress is not linear with the strain– was chosen to highlight the robustness of the solution. Considering this, the control strategy also shows a first-order-like behaviour both before and after the initial contact and reaches the goal position without significant error in the contact direction, Y. Moreover, it is worth noting that both the perpendicular-to-penetration position, X, and the direction angle, α, show error peaks during this operation but both are corrected while pushing the foam. Meanwhile, the adaptive parameters evolve during the operation, being their steepest change when the RM stalled its advance at 5 s.

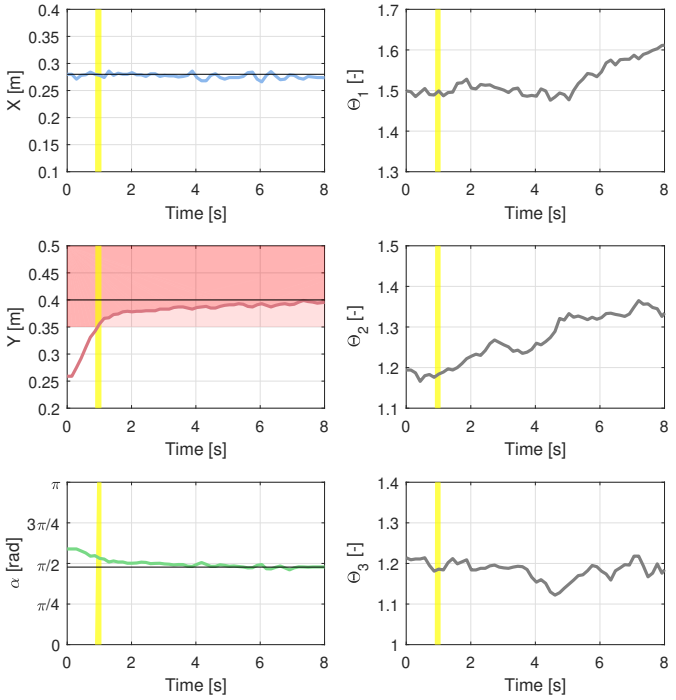

Fig. 9. EE position and adaptive parameters for the contact scenario, with the foam in red (lighter for the area already pushed and darker for the remaining) and the initial contact in yellow.

VI. Conclusions

An nonlinear and adaptive solution for low-cost compliant lightweight manipulation is presented, addressing the accuracy-reducing second-order oscillations and improving the robustness of the system. Theoretical stability analysis and experimental results studying the behaviour of the solution are provided. Among the latter, the solution is evaluated in both impact and contact scenarios, demonstrating enhanced disturbance rejection capabilities and zero steady-state error, respectively. Finally, the implementation of the solution in an aerial inspection mission and the subsequent experimental results are left as future work.

Acknowledgement

The authors gratefully acknowledge to the engineer in Mechatronics Jesús Tormo, as member of GRVC, for the design and construction of the experimental setup [30].

REFERENCES

[1] A. Suarez, G. Heredia, and A. Ollero, "Lightweight compliant arm for aerial manipulation," in *2015 IEEE/RSJ International Conference on Intelligent Robots and Systems (IROS)*, Sep. 2015, pp. 1627–1632.

[2] A. Suarez, P. R. Soria, G. Heredia, B. C. Arrue, and A. Ollero, "Anthropomorphic, compliant and lightweight dual arm system for aerial manipulation," in *2017 IEEE/RSJ International Conference on Intelligent Robots and Systems (IROS)*, Sep. 2017, pp. 992–997.

[3] A. Suarez, A. E. Jimenez-Cano, V. M. Vega, G. Heredia, A. Rodriguez-Castaño, and A. Ollero, "Design of a lightweight dual arm system for aerial manipulation," *Mechatronics*, vol. 50, pp. 30 – 44, 2018. [Online]. Available: http://www.sciencedirect.com/science/article/pii/S0957415818300011

[4] M. Quigley, A. Asbeck, and A. Ng, "A low-cost compliant 7-DOF robotic manipulator," in *2011 IEEE International Conference on Robotics and Automation (ICRA)*, May 2011, pp. 6051–6058.

[5] A. Jain and C. C. Kemp, "Pulling open doors and drawers: Coordinating an omni-directional base and a compliant arm with equilibrium point control," in *2010 IEEE International Conference on Robotics and Automation (ICRA)*, May 2010, pp. 1807–1814.

[6] L. Baccelliere, N. Kashiri, L. Muratore, A. Laurenzi, M. Kamedula, A. Margan, S. Cordasco, J. Malzahn, and N. G. Tsagarakis, "Development of a human size and strength compliant bi-manual platform for realistic heavy manipulation tasks," in *2017 IEEE/RSJ International Conference on Intelligent Robots and Systems (IROS)*, Sep. 2017, pp. 5594–5601.

[7] R. C. Luo, Y.W. Perng, B.H. Shih, and Y.H. Tsai, "Cartesian position and force control with adaptive impedance/compliance capabilities for a humanoid robot arm," in *2013 IEEE International Conference on Robotics and Automation (ICRA)*, May 2013, pp. 496–501.

[8] A. Suarez, G. Heredia, and A. Ollero, "Physical-virtual impedance control in ultralightweight and compliant dual-arm aerial manipulators," *IEEE Robotics and Automation Letters (RA-L)*, vol. 3, no. 3, pp. 2553–2560, July 2018.

[9] F. Ficuciello, L. Villani, and B. Siciliano, "Variable impedance control of redundant manipulators for intuitive human–robot physical interaction," *IEEE Transactions on Robotics*, vol. 31, no. 4, pp. 850–863, Aug 2015.

[10] A. Colomé, D. Pardo, G. Alenyà, and C. Torras, "External force estimation during compliant robot manipulation," in *2013 IEEE International Conference on Robotics and Automation (ICRA)*, May 2013, pp. 3535–3540.

[11] A. D. Luca, A. Albu-Schaffer, S. Haddadin, and G. Hirzinger, "Collision detection and safe reaction with the DLR-III lightweight manipulator arm," in *2006 IEEE/RSJ International Conference on Intelligent Robots and Systems (IROS)*, Oct 2006, pp. 1623–1630.

[12] A. Suarez, A. M. Giordano, K. Kondak, G. Heredia, and A. Ollero, "Flexible link long reach manipulator with lightweight dual arm: Soft-collision detection, reaction, and obstacle localization," in *2018 IEEE International Conference on Soft Robotics (RoboSoft)*, April 2018, pp. 406–411.

[13] A. Suarez, G. Heredia, and A. Ollero, "Lightweight compliant arm with compliant finger for aerial manipulation and inspection," in *2016 IEEE/RSJ International Conference on Intelligent Robots and Systems (IROS)*, Oct 2016, pp. 4449–4454.

[14] T. Lens and O. von Stryk, "Design and dynamics model of a lightweight series elastic tendon-driven robot arm," in *2013 IEEE International Conference on Robotics and Automation (ICRA)*, May 2013, pp. 4512–4518.

[15] D.Rus and M. Tolley, "Design, fabrication and control of soft robots," *Nature*, vol. 521, pp. 467–475, 2015.

[16] "AEROARMS project: AErial RObotic system integrating multiple ARMS and advanced manipulation capabilities for inspection and maintenance," http://www.aeroarms-project.eu/, European Commission under the H2020 Framework Programme.

[17] A. Marter, A. Dickinson, F. Pierron, and M. Browne, "A practical procedure for measuring the stiffness of foam like materials," *Experimental Techniques*, vol. 42, no. 4, pp. 439–452, Aug 2018. [Online]. Available: https://doi.org/10.1007/s40799-018-0247-0

[18] J.M. Dulieu-Barton, C. Boyenval Langlois, O.T. Thomsen, S. Zhang, and R.K. Fruehmann, "Derivation of temperature dependent mechanical properties of polymer foam core materials using optical extensometry," *EPJ Web of Conferences*, vol. 6, p. 38004, 2010. [Online]. Available: https://doi.org/10.1051/epjconf/20100638004

[19] L. Roveda, N. Pedrocchi, F. Vicentini, and L. M. Tosatti, "An interaction controller formulation to systematically avoid force overshoots through impedance shaping method with compliant robot base," *Mechatronics*, vol. 39, pp. 42 – 53, 2016. [Online]. Available: http://www.sciencedirect.com/science/article/pii/S0957415816300769

[20] G. Antonelli, S. Chiaverini, and G. Fusco, "A new on-line algorithm for inverse kinematics of robot manipulators ensuring path tracking capability under joint limits," *IEEE Transactions on Robotics and Automation*, vol. 19, no. 1, pp. 162–166, February 2003.

[21] P. Falco and C. Natale, "On the stability of closed-loop inverse kinematics algorithms for redundant robots," *IEEE Transactions in Robotics*, vol. 27, no. 4, pp. 780–784, August 2011.

[22] M. I. Sánchez, J. Á. Acosta, and A. Ollero, "Integral action in first-order closed-loop inverse kinematics. application to aerial manipulators," in *Robotics and Automation (ICRA), 2015 IEEE International Conference on*, May. 26-30 2015, pp. 5297–5302.

[23] B. Siciliano, "Parallel force and position control of flexible manipulators," *Control Theory and Applications, IEEE*, 2000. [Online]. Available: http://ieeexplore.ieee.org/xpls/abs{_}all.jsp?arnumber=903453

[24] B. Siciliano and L. Villani, "An inverse kinematics algorithm for interaction control of a flexible arm with a compliant surface," *Control Engineering Practice*, vol. 9, no. 2, pp. 191–198, 2001.

[25] Y. Pan, H. Wang, X. Li, and H. Yu, "Adaptive command-filtered backstepping control of robot arms with compliant actuators," *IEEE Transactions on Control Systems Technology*, vol. 26, no. 3, pp. 1149–1156, May 2018.

[26] K. P. Tee, R. Yan, and H. Li, "Adaptive admittance control of a robot manipulator under task space constraint," in *2010 IEEE International Conference on Robotics and Automation*, May 2010, pp. 5181–5186.

[27] S. Chiaverini, G. Oriolo, and I. Walker, "Kinematically redundant manipulators," in *Handbook of Robotics*. Berlin Heidelberg: Springer, 2008, pp. 245–268.

[28] B. Siciliano, L. Sciavicco, L. Villani, and G. Oriolo, *Robotics. Modelling, planning and control*. Springer-Verlag (UK), 2009.

[29] C. Della Santina, M. Bianchi, G. Grioli, F. Angelini, M. Catalano, M. Garabini, and A. Bicchi, "Controlling soft robots: Balancing feedback and feedforward elements," *IEEE Robotics Automation Magazine*, vol. 24, no. 3, pp. 75–83, Sep. 2017.

[30] J. Tormo-Barbero, "Diseño y control de un robot manipulador," Master's thesis, Escuela Técnica Superior de Ingeniería, Universidad de Sevilla, 2018.

[31] Robotis, "Dynamixel AX Series," http://www.robotis.us/ax-series/, online; accessed 11 January 2019.

[32] Vanadium Labs, "ArbotiX-M Robocontroller," http://www.vanadiumlabs.com/arbotix, online; accessed 11 January 2019.